Fuel 294 (2021) 120538

Contents lists available at ScienceDirect

Fuel

journal homepage: www.elsevier.com/locate/fuel

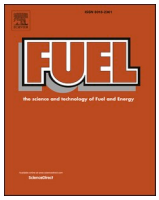

Full Length Article

Experimental study on NO_x emissions of pulverized coal combustion preheated by a 2 MW novel self-sustained preheating combustor

Ziqu Ouyang [a,b], Wenhao Song [a,b], Jingzhang Liu [a,*], Jianguo Zhu [a,b], Chengbo Man [a], Shujun Zhu [a,c], Hongliang Ding [a,b]

[a] Institute of Engineering Thermophysics, Chinese Academy of Sciences, Beijing 100190, China
[b] University of Chinese Academy of Sciences, Beijing 100049, China
[c] Institute of Mechanics, Chinese Academy of Sciences, Beijing 100190, China

ARTICLE INFO

Keywords:
Self-sustained preheating combustion
Air staging
NO_x emission
Pulverized coal

ABSTRACT

In the study, a potentially feasible low-NO_x combustion technology, based on self-sustained preheating combustion of pulverized coal, is proposed. A 2 MW novel self-sustained preheating combustion test rig was employed, and bituminous coal was used in the experiment. A novel internal fluidized bed combustor (IFBC) was used as the preheating chamber for pulverized coal, followed by air staging in the combustion chamber. Preheating characteristics of the IFBC and the temperature distribution in the primary combustion zone were discussed. Next, the effects of the air staging ratio of the preheated fuel burner and the positions of tertiary air on the combustion characteristics and NO_x emissions of bituminous coal were investigated. The results demonstrated that pulverized coal led to a clean and efficient operation, producing a minimum NO_x emission of 72 mg/Nm^3 (@ 6% O_2). The fuel could be preheated to above 900 °C stably, and the obtained conversion rate of fuel-bound N (fuel-N) was up to 80.2% in the IFBC. Moreover, the temperature profile in the primary combustion zone exhibited a symmetrical distribution along the central axis of the preheated fuel burner. The high-temperature primary combustion zone moved upward with increasing air staging ratio of the preheated fuel burner, and a region with low oxygen and strong reducibility was formed, inhibiting NO_x generation. To maximally reduce NO_x emission, a large retention time in the reducing zone and uniform mixing of reactants were crucial. The multi-layer arrangement and delayed supply of tertiary air were found to be conducive to significantly reducing NO_x emissions.

1. Introduction

Nitrogen oxides (NO_x) can cause severe environmental issues such as acid deposition, ozone depletion, and photochemical smog; hence, NO_x emissions, including those from coal-fired power plants, represent a major environmental concern. The reduction of NO_x emissions is currently one of the major challenges for environmental protection. Strict standards have been implemented worldwide to reduce NO_x emissions from coal-fired power plants. China has promulgated ultra-low pollutant emission standards since 2014, restricting NO_x emissions to < 50 mg/Nm^3 at 6% O_2 for coal-fired boilers [1]. The NO_x emission limit for coal-fired power plants over 500 MWe has been set to 200 mg/Nm^3 at 6% O_2 by the European Union since 2016 [2]. Accordingly, rigorous requirements have been proposed for the clean combustion of coal.

Over the past few years, extensive efforts have been made to develop novel technologies that restrict NO_x emissions, including air staging combustion [3-5], low-NO_x burners [6,7], selective catalytic reduction (SCR), and selective non-catalytic reduction (SNCR) [8,9]. SCR and SNCR involve the addition of nitrogen reducing agents, thereby significant denitrification; however, they exhibit limitations such as high economic cost, ammonia leak, and catalyst pollution [9,10]. Combined technologies based on air staging combustion and low-NO_x burners have been extensively used to control NO_x emissions in coal-fired power plants, because they are the most direct and economical option for NO_x reduction.

Two methods of air staging in a coal-fired boiler were summarized by Van Der Lans [11]. One is the internal air staging, which is also known as burner air staging. Through specific air staging in low-NO_x burners, fuel-rich zones involving devolatilization are created close to the exits of the burners. These zones can inhibit fuel-NO_x conversion, promoting NO_x

* Corresponding author.
E-mail address: liujingzhang@iet.cn (J. Liu).

https://doi.org/10.1016/j.fuel.2021.120538
Received 9 December 2020; Received in revised form 20 February 2021; Accepted 20 February 2021
Available online 12 March 2021

Nomenclature

F_p	primary air flow rate, Nm^3/h
F_{in}	inner secondary air flow rate, Nm^3/h
F_{out}	outer secondary air flow rate, Nm^3/h
F_t	tertiary air flow rate, Nm^3/h
F_{stoi}	the stoichiometric air flow rate for complete combustion, Nm^3/h
a_1	the ash content in the fuel
a_2	the ash content in the preheated fuel
C_{fa}	the combustible content in exit fly ash
C_X	the conversion ratios of components in the fuel, %
η	combustion efficiency, %
q_g	the heat loss due to incomplete gaseous combustibles, %
q_s	the heat loss due to incomplete combustion of solid combustibles, %
λ	the equivalence ratio of total air
λ_p	the equivalence ratio of primary air
λ_s	the equivalence ratio of secondary air
λ_t	the equivalence ratio of tertiary air
M_{io}	the momentum ratio of inner secondary air to outer secondary air
v_{in}	inner secondary air velocity, m/s
v_{out}	outer secondary air velocity, m/s
x_1	the component X (C, H, volatile, and so on) content in the fuel
x_2	the component X (C, H, volatile, and so on) content in the preheated fuel
$Q_{net,ar}$	the net calorific value of the fuel as received
A_{ar}	the ash mass fraction of the fuel as received
CO	the volumetric percentages of CO in dry flue gas
RO_2	the volumetric percentage of tri-atomic gas in dry flue gas

reduction in the flame. Currently, a range of mature and reliable low-NO_x burners with wide applications have been developed (e.g., LNASB burner [6], HT-NR burner [7], PM burner [12], CFR burner [13], and petal swirl burner [14]). The other method is external air staging, also termed as furnace air staging, in which combustion air is added as over-fire air (OFA) above the burner belt. This can decrease the oxygen concentration in the primary combustion zone. Hence, nitrogen intermediates (HCN and NH_3) tend to react with NO to form N_2 instead of reacting with O_2 to form NO. Furnace air staging technology can significantly reduce NO_x emissions. Several studies on the topic have been reported, including those conducted by Choi [15,16], Fan [17,18], Kuang [19], and Zha [20] among others.

A gas fire coal heating technology developed by the All Russian Thermal Engineering Institute [4,21] has been demonstrated to deliver highly efficient and clean use of pulverized coal. Its essence is that substantial fuel-bound N (fuel-N) was easy to convert into N_2 in a preheating chamber under a highly reducing atmosphere, which could restrict NO_x generation at the source. However, the pulverized coal was preheated by the hot flue gas generated from natural gas combustion, whose economic cost was high. According to the coal preheating combustion technology developed by the Institute of Engineering Thermophysics, Chinese Academy of Sciences [22], the pulverized coal was initially preheated to above 850 °C in a circulating fluidized bed (CFB) through itself pyrolysis, gasification, and combustion at a low air ratio, and then entered the combustion chamber to be further combusted with air staging method. A 30 kW test rig and a 0.2 MW test rig were set up successively, and a series of mechanism studies and engineering applications were conducted [23-26]. Ouyang investigated the process of anthracite preheating and NO_x formation mechanism in a 30 kW test rig [24]. Zhu focused on the pattern of NO_x emissions obtained using different coal types and nozzle structures [25]. Liu reported the flame pictures in the combustion chamber [26]. In Man's research, the effects of air ratio in CFB and air distribution on the combustion and NO_x emission characteristics were investigated in a 0.2 MW test rig [23]. Therein, a high combustion efficiency and low NO_x emissions were implemented simultaneously using coal preheating combustion technology. Nevertheless, some potential defects were identified in the CFB, such as large size, high engineering cost, and complicated structure). A novel self-sustained preheating combustion technology was developed, to operate an internal fluidized bed combustor (IFBC) as the preheating chamber for pulverized coal [27]. Compared with the CFB, the conventional loop seal was removed, while the gas–solid separator and the dipleg were installed in the riser of the IFBC. This combustion system exhibited a simple and compact structure, facile operation, and low heat dissipation. Combining the IFBC with the air staging method, the novel self-sustained preheating combustion technology can be applied in conventional pulverized coal boilers or even in coal-fired power plants to attain acceptable results (Fig. 1). In existing studies, preheating characteristics of the IFBC have not been systematically characterized, and the synergetic effects of the IFBC and air staging on NO_x emissions remains unclear.

In this study, bituminous coal was used in a 2-MW novel self-sustained preheating combustion test rig. Preheating characteristics of the IFBC including pressure drop, temperature variations, and the analysis of high-temperature coal gas and semi-coke were investigated. In addition, the temperature profile in the primary combustion zone was analyzed. Furthermore, the effects of the air staging ratio of the preheated fuel burner and the position of tertiary air on the combustion characteristics and NO_x emissions using bituminous coal were investigated. The aim was to formulate the control strategy for low NO_x emissions by adopting self-sustained preheating combustion technology, which can effectively guide its industrial application.

2. Experimental

2.1. Fuel characteristics

The proximate and ultimate analysis of Shenmu bituminous coal used in the experiment are listed in Table 1. The nitrogen mass concentration in this representative bituminous coal was 0.98% and the volatile matter was 30.57%. The coal particle size distribution (PSD) ranged from 0.1 μm to 136 μm (Fig. 2). The mass fraction for the minimum particle size (d_5), average particle size (d_{50}), and maximum particle size (d_{90}) are 3, 31, and 89 μm, respectively. The PSD of the fuel was consistent with that used in conventional pulverized coal boilers [16,28]. In addition, fuel with a particle size of 100–400 μm has been

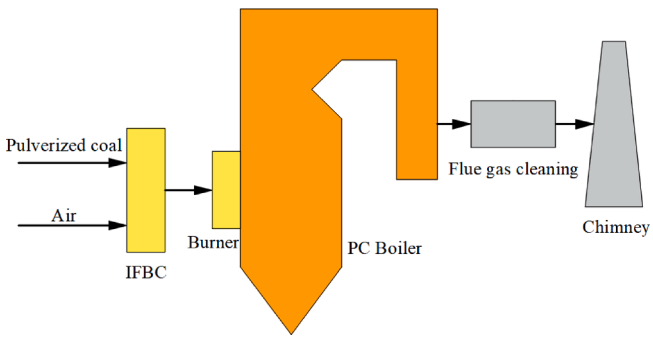

Fig. 1. Schematic diagram of novel self-sustained preheating combustion technology applied to PC boilers.

Table 1
The ultimate and proximate analysis of Shenmu bituminous coal.

Items	Data
Ultimate analysis (wt%, air- received basis)	
Carbon	62.94
Hydrogen	3.88
Oxygen	10.18
Nitrogen	0.98
Sulfur	0.40
Proximate analysis (wt%, air-dried basis)	
Moisture	11.80
Ash	9.82
Volatile matter	30.57
Fixed carbon	47.80
Low heating value (MJ/kg)	24.43

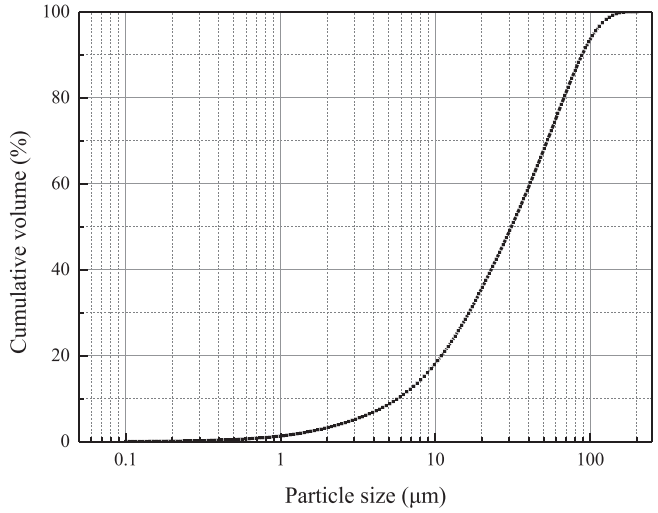

Fig. 2. Particle size distribution of Shenmu bituminous coal.

characterized previously [24,25], and the experimental systems exhibited a stable operation.

2.2. Apparatus and methods

A schematic of the 2 MW novel self-sustained preheating combustion test rig is illustrated in Fig. 3. This combustion system consisted of an IFBC, a combustion chamber, a gas cooler, and other auxiliary devices. The designed thermal power was 2 MW, and the feeding fuel rate was approximately 0.3 t/h.

Fig. 4 presents the schematic diagram of the IFBC. The IFBC was made of stainless steel (length: 2200 mm; inner diameter (I.D.): 450 mm) and lined with refractory fiber. As mentioned earlier, a gas–solid separator and a dipleg were installed in the riser. The IFBC was equipped with an ignition oil burner to achieve initial heating and fuel ignition. Prior to conducting the experiments, 70 kg of quartz sand (0.1–1.2 mm) was added to the IFBC as the bed material for stable circulation. The pulverized coal was fed into the IFBC by the powder feeding air. Fluidized air was supplied from the bottom of the IFBC. The test rig started with the heating stage, where the fuel was led into the IFBC gradually and burned completely to heat the IFBC and bed material. As the temperature of the IFBC increased up to 800 °C, the combustion condition switched to the test condition. The air equivalence ratio of the primary air (PA) including fluidized air and powder feeding air, was approximately 0.2. The IFBC could run steadily without auxiliary heating and sustain itself in the range of 850–950 °C by the heat released from partial pyrolysis, gasification, and combustion of the fuel. It is worth noting that, the gasification reaction was dominant, and the pulverized coal was converted into high-temperature coal gas and semi-coke, which were defined as the preheated fuel. The high-temperature semi-coke circulated in the IFBC; once the particle size was sufficiently small, after physical breakage and chemical reactions, it escaped from the gas–solid separator.

The preheated fuel was injected from the bottom of the combustion chamber. The combustion chamber was 15000 mm in height and divided into two vertical parts. The bottom part had a water wall, with a height of 4000 mm and a cross-sectional area of 800 × 800 mm^2. The top part (11000 mm) was lined with the refractory material with a cross-sectional area of 1000 × 1000 mm^2. The nozzle structure of the coaxial jet was adopted in the preheated fuel burner, where the preheated fuel was surrounded by the inner secondary air (ISA) and outer secondary air (OSA) (Fig. 5). The pipe diameters of preheating fuel, ISA, and OSA were 119, 144, and 174 mm, respectively. Different from the fuel used in the conventional burner, the preheated fuel from IFBC was the high-temperature coal gas and semi-coke. Five tertiary air nozzles (nozzles 1–5) were installed along the sidewalls and arranged at 2600, 5500, 8200, 10700, and 13200 mm from the bottom of the combustion chamber, respectively; the air was injected into the combustion chamber horizontally via these nozzles. The flue gas was discharged into the atmosphere through a chimney after passing through the gas cooler and bag filter.

A programmable logic controller was applied in this test rig for measurement and control. The flow rates of powder feeding air, fluidized air, ISA, OSA, and tertiary air were regulated and measured using flow meters. The differential pressures of the dense phase zone and dilute phase zone in the riser were measured using three pressure transducers arranged at 250, 1100, and 2100 mm from the bottom of the IFBC, respectively. Two thermocouples were arranged at 1100 mm and 2100 mm from the bottom of the IFBC, respectively, and one was arranged at the outlet of the IFBC. Fifteen thermocouples were arranged along the center of the combustion chamber at a distance of 460, 770, 1060, 1570, 2370, 3350, 4380, 5360, 6360, 7380, 8860, 10400, 11900, 13400, and 14400 mm from the bottom of the combustion chamber, respectively. The dotted lines in the combustion chamber represented the cross section of gird temperature measured, which were arranged at 650, 950, 1100, 1650, 2050, 2300, 2550 mm from the bottom of the combustion chamber. Moreover, all the thermocouples were calibrated, and the absolute error of the measured data was < 1%. The sampling point of the high-temperature coal gas and semi-coke was set at the outlet of the IFBC. The sampling point of fly ash and flue gas was set at the inlet of the bag filter. Furthermore, a Fourier transform infrared (FT-IR) gas analyzer (Gasmet DX-4000) and a zirconia oxygen analyzer were used to analyze the flue gas components. The errors in gas concentrations were ± 2%.

2.3. Experimental conditions

The experimental conditions are presented in Table 2. λ_p, λ_s, λ_t, λ are denoted as the air equivalence ratio of primary air, secondary air, tertiary air, and total air, respectively. M_{io} is defined as the momentum ratio of ISA to OSA, a dimensionless parameter used to evaluate the air staging ratio of preheated fuel burner. These parameters are defined as follows:

$$\lambda_p = \frac{F_p}{F_{\mathrm{Stoi}}} \tag{1}$$

$$\lambda_s = \frac{F_{\mathrm{in}} + F_{\mathrm{out}}}{F_{\mathrm{Stoi}}} \tag{2}$$

$$\lambda_t = \frac{F_t}{F_{\mathrm{Stoi}}} \tag{3}$$

$$\lambda = \frac{F_p + F_{\mathrm{in}} + F_{\mathrm{out}} + F_t}{F_{\mathrm{Stoi}}} \tag{4}$$

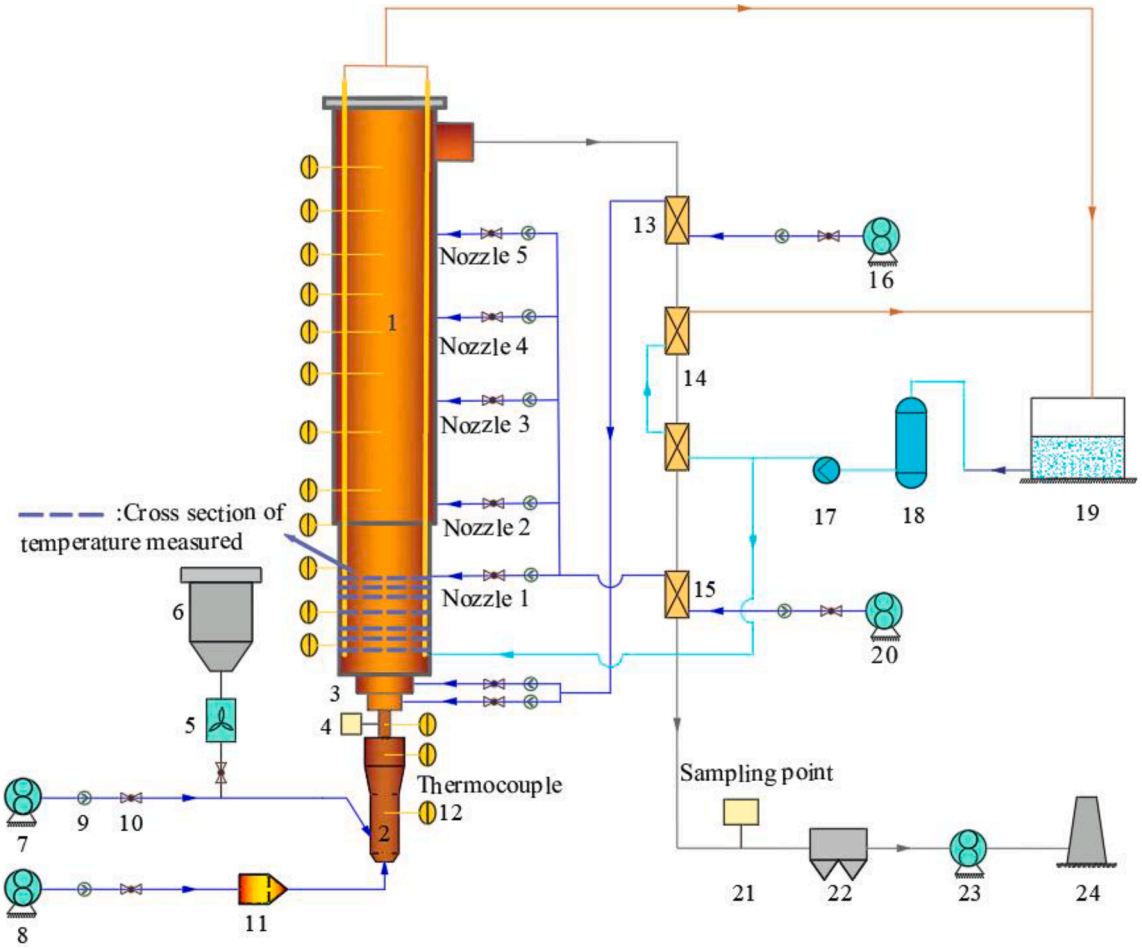

Fig. 3. Schematic diagram of the 2 MW novel self-sustained preheating combustion test rig: 1, Combustion chamber; 2, IFBC; 3, Preheated fuel burner; 4, Sampling point of preheated fuel; 5, Fuel conveyor; 6, Fuel bunker; 7, Powder feeding air fan; 8, Fluidized air fan; 9, Flow meter; 10, Valve; 11, Ignition oil burner; 12, Thermocouple; 13, Secondary air preheater; 14, Flue gas cooler; 15, Tertiary air preheater; 16, Secondary air fan; 17, Pump; 18, Cooling water tower; 19, Cooling water tank; 20, Tertiary air fan; 21, Sampling point of flue gas and fly ash; 22, Bag filter; 23, Induced fan; 24, Chimney.

$$M_{io} = \frac{F_{\text{in}} v_{\text{in}}}{F_{\text{out}} v_{\text{out}}} \tag{5}$$

where F_{stoi} is the stoichiometric air flow rate for complete combustion of the fuel, F_{p} is the PA flow rate (including powder feeding air and fluidized air), F_{s} is the secondary air flow rate (including ISA and OSA), and F_{t} is the tertiary air flow rate. F_{in}, F_{out}, v_{in}, and v_{out} are the ISA flow rate, OSA flow rate, ISA velocity, and OSA velocity, respectively.

According to Table 2, the temperature profile in the primary combustion zone was investigated considering Case 1. The effects of M_{io} (cases 2–4) and tertiary air positions (cases 5–8) on the combustion characteristics and NO_x emissions were investigated. After preheating, the operating temperatures of the OSA, ISA, and tertiary air throughout the experiment were approximately 200, 250, and 70 °C, respectively. The thermal power, λ_{p}, λ, and the operating temperatures of the OSA, ISA, and tertiary air varied slightly owing to adjustments on the operating conditions, so the variations were considered negligible.

Table 3 shows the retention times for different sections of the experiment. t_{i}, t_1, t_2, t_3, t_4, t_5, and t_6 are denoted as the retention times in the IFBC, combustion chamber bottom to nozzle 1, combustion chamber bottom to nozzle 2, combustion chamber bottom to nozzle 3, combustion chamber bottom to nozzle 4, combustion chamber bottom to nozzle 5, and combustion chamber bottom to its outlet, respectively.

3. Results and discussion

3.1. Preheating characteristics in the IFBC

Fig. 6 presents the temperature variations when switching between combustion condition and preheating condition. During combustion, stable circulation was maintained in the IFBC with fluidized air, and the temperature increased up to 850 °C through the combustion of Shenmu bituminous coal. Subsequently, the pulverized coal was fed into the IFBC through powder feeding air. First, the temperature of the IFBC increased rapidly and then decreased, until it eventually stabilized. The fluctuation of temperature might have been related to delays in the fuel feed. Because of the low air equivalence ratio, the temperature in the IFBC stabilized at approximately 930 °C under the partial pyrolysis, gasification, and combustion of the pulverized coal.

Pressure drop and temperature variations were recorded over time at the stable condition in Case 1, as illustrated in Figs. 7 and 8, respectively. The average temperatures at 1100 mm, that at 2100 mm from the bottom of the riser, and that at the outlet of the IFBC were 929, 925, and 916 °C, respectively, and the corresponding temperature difference was < 15 °C. In addition, the pressure fluctuation was steady, and the temperature profile was uniform in the IFBC. This indicated that good fluctuation and a stable circulation loop were set up in the IFBC. Furthermore, both the thermal power and λ_{p} affected the preheating temperature of the IFBC, which was a crucial factor for the preheated fuel [24]. The experiment was performed for 24 h till it was complete for

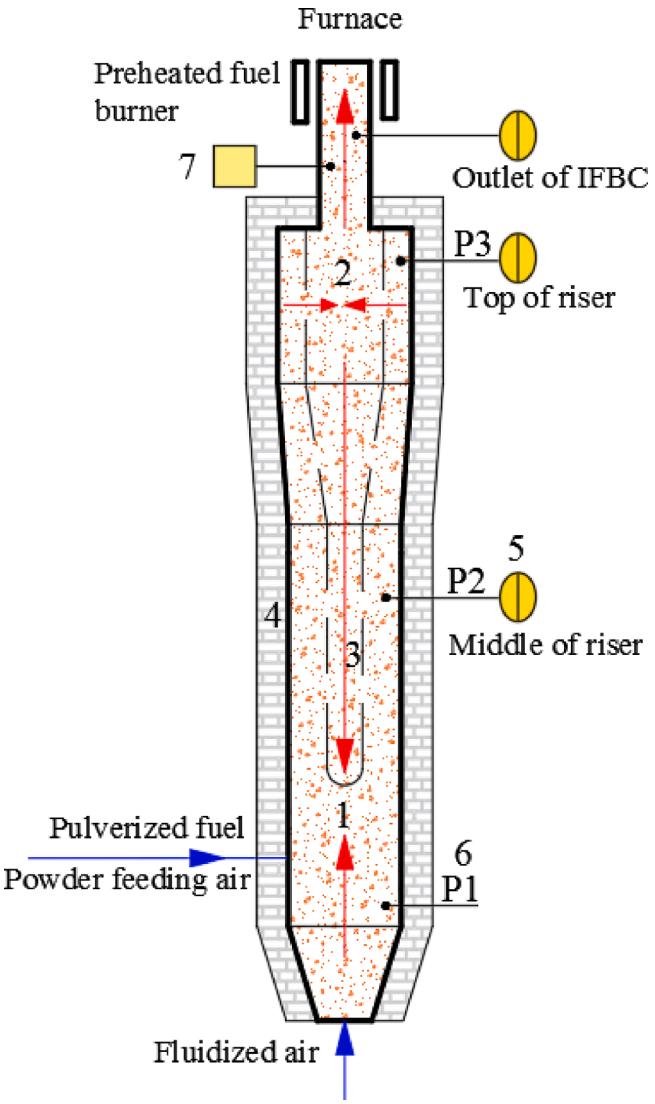

Fig. 4. Schematic diagram of the IFBC: 1, Riser; 2, Gas-solid separator; 3, Dipleg; 4, Ceramic fiber; 5, Thermocouple; 6, Pressure transducer; 7, Sampling point of preheated fuel.

all cases, and the preheating temperature exhibited slight fluctuations from 920 to 940 °C in the IFBC. It could be assumed that the properties of the preheated fuel were almost constant in all cases, not being affected by thermal power as well as λ_p variations. In brief, the IFBC could be able to preheat the pulverized coal up to 900 °C steadily and continuously, which complied with the requirement of self-sustained preheating combustion technology.

To determine the preheating characteristics, high-temperature coal gas and semi-coke were sampled at the outlet of the IFBC. Table 4 presents the analysis of high-temperature coal gas, which was mainly composed of N_2, H_2, CO, CH_4, and CO_2 (average volume fractions of 69.89, 10.93, 12.21, 3.01, and 3.85%, respectively). Consistent results for the analysis of high-temperature coal gas analysis were reported in refs [25,29]. Because of the low air equivalence ratio, a strongly reducing atmosphere prevailed and O_2 was not detected in the IFBC. The combustible gases mainly comprised H_2, CO, and CH_4, with a low heating value of 4.36 MJ/Nm^3, facilitating rapid ignition and stable combustion of the preheated fuel in the combustion chamber. Notably, a considerable amount of reducing gas generated in the IFBC (i.e., H_2, CO, and C_nH_m) was conducive to reducing NO_x.

Table 5 lists the proximate and ultimate analysis of the high-temperature semi-coke. To evaluate the conversion performance of the

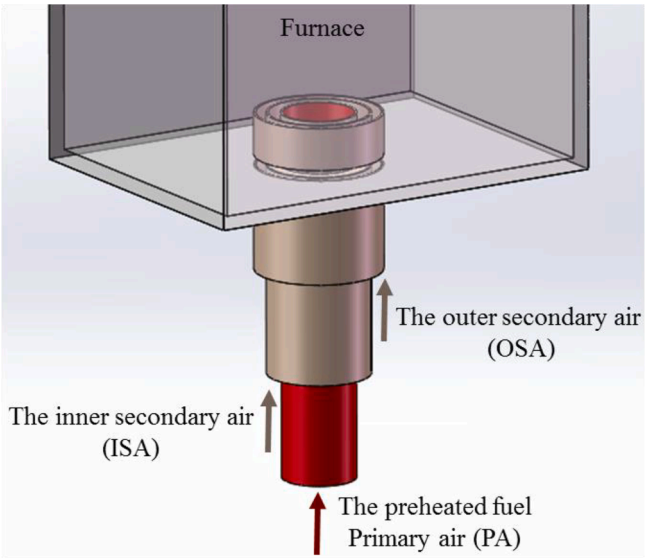

Fig. 5. Schematic diagram of the preheated fuel burner.

pulverized coal particles in the IFBC, the conversion rate of each component was calculated (Table 5). According to the ash balance [24], the conversion ratio of component × (C_x) during the preheating process is defined as follows:

$$C_x = 1 - \frac{a_1 \times x_2}{a_2 \times x_1}(\%) \quad (6)$$

where a_1 and x_1 are the fractions of the ash and component × (e.g., C, H, volatiles) in the fuel, respectively. a_2 and x_2 are the fractions of the ash and component × in the high-temperature semi-coke, respectively.

As shown in Table 4, 97.8% of volatile matter and 49.6% of fixed carbon were released during the preheating process. This indicated that nearly all the volatile matter and half of the fixed carbon were converted to release heat, which maintained the overall thermal balance of the IFBC. The conversion rates of C, H, and O were 68.9, 85.9, and 78.5%, respectively. Moreover, the conversion rate of fuel-N composed of volatile-N and char-N was 80.2%. Among them, volatile-N was almost completely released and the residual N entered the combustion chamber to burn in the form of char-N. In the study reported by Ouyang and Zhu [30,31], fuel-N was converted into N_2, HCN, NH_3 in the preheating chamber; therein, N was largely reduced to inert N_2. The conversion rate of elemental N in the IFBC was higher than that in the CFB, which facilitated the reduction of NO_x emissions. Notably, the conversion rate of S was only 11.5%, considerably lower than that of other components, and a similar result was reported by Zhang [32]. The low S-conversion rate may be explained as follows: Organic sulfur in the fuel was stable which hindered the release of S [33]. In addition, the fluidized bed combustion had a strong capability for sulfur self-retention. In that case, S might have been partially retained in the form of solid compounds in the ash by combining with coal calcium to form CaS or $CaSO_4$ [34]. Thus far, the conversion mechanisms of N and S during the preheating process have not been thoroughly addressed; these can be affected by several factors, such as coal composition, reaction temperature, gas–solid mixing, retention time, and the atmosphere in the IFBC. Additional studies on the transformation mechanisms that occur in the IFBC will be conducted in the future.

3.2. *Temperature profile in the primary combustion zone.*

The preheated fuel was fed into the combustion chamber directly via the preheated fuel burner and burned using the air staging method. The secondary air provided oxygen for early-stage combustion. Tertiary air was supplied at a location above 2600 mm from the bottom of the

Table 2
Operating conditions of the experiment.

Items	Case 1	Case 2	Case 3	Case 4	Case 5	Case 6	Case 7	Case 8
Thermal power (MW)	1.88	2.08	1.76	1.88	1.84	1.83	1.87	1.92
λ_p	0.18	0.16	0.20	0.18	0.19	0.19	0.18	0.18
λ_s	0.45	0.66	0.79	0.74	0.53	0.54	0.52	0.51
M_{io}	0.23	0.22	0.39	0.62	0.42	0.41	0.42	0.41
F_{in} (Nm^3/h)	215	345	431	494	310	308	306	305
F_{out} (Nm^3/h)	569	934	870	797	605	605	600	604
F_t (Nm^3/h)	926	829	634	648	993	978	889	938
v_{in} (m/s)	20.6	33.1	41.3	47.4	29.7	29.5	29.3	29.3
v_{out} (m/s)	34.1	55.9	52.1	47.7	36.2	36.2	35.9	36.2
Tertiary air position	4,5	4	4	4	2,3	3,4	4,5	5
λ_t	0.57	0.43	0.39	0.37	0.58	0.58	0.51	0.53
λ	1.20	1.25	1.38	1.29	1.30	1.31	1.21	1.22

Table 3
Retention times of different sections in the experiment.

Retention time (s)	Case 1	Case 2	Case 3	Case 4	Case 5	Case 6	Case 7	Case 8
t_i	0.79	0.79	0.76	0.80	0.79	0.79	0.80	0.78
t_1	0.13	0.12	0.11	0.12	0.13	0.13	0.13	0.13
t_2	2.46	1.87	1.83	1.87	2.25	2.26	2.27	2.25
t_3	5.07	3.84	3.77	3.85	3.76	4.66	4.68	4.64
t_4	7.93	6.07	5.96	6.09	5.22	6.30	7.10	7.05
t_5	9.84	7.44	7.46	7.60	6.68	7.62	8.81	9.59
t_6	10.80	8.38	8.49	8.64	7.72	8.52	9.69	10.44

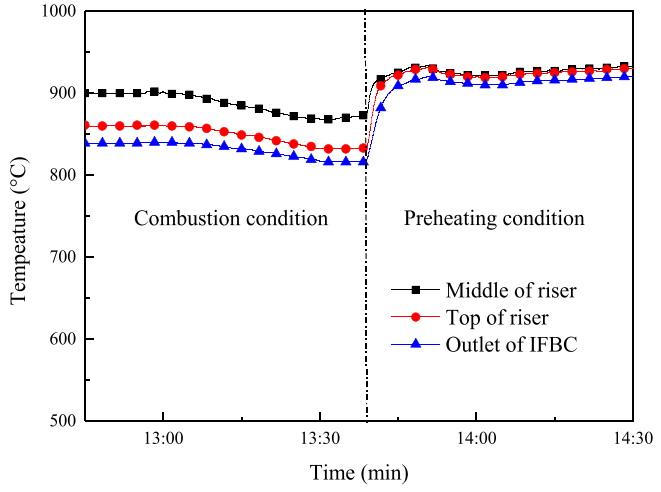

Fig. 6. Temperature variations under the switch of combustion condition and preheating condition.

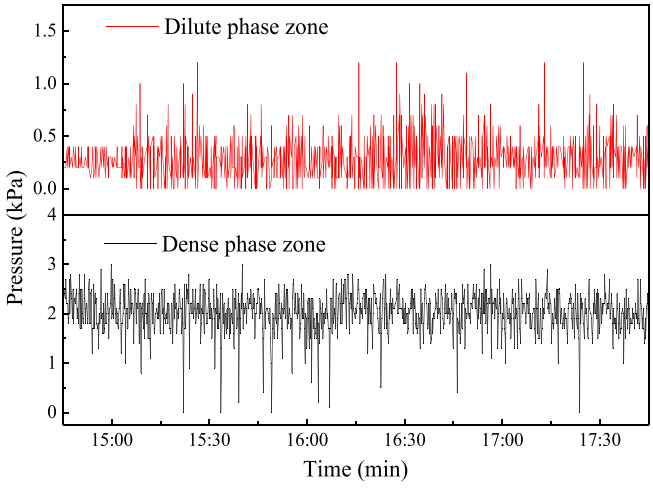

Fig. 7. Pressure drop variations with time in the IFBC.

combustion chamber for complete combustion. The preheated fuel was composed of high-temperature coal gas and semi-coke, which differed from the raw coal. Because the temperature of the preheated fuel was higher than the kindling point of the Shenmu bituminous coal (349 °C) measured by thermogravimetry, the fuel was rapidly ignited to maintain stable combustion. In addition, it was reported that the pore volume and specific surface area of the high-temperature semi-coke increased, whereas its particle size decreased [24], which accelerated the involved chemical reactions. Thus, the process was different from the conventional combustion methods, which required "three high zones" (high temperature, high fuel concentration, and high oxygen concentration) for ignition and stable combustion.

To determine the combustion characteristics at the early-stage combustion, a thermocouple was manually inserted into the primary combustion zone to conduct grid temperature measurement during the stable condition in Case 1. Fig. 9 shows the temperature points on the cross section of the combustion chamber. The temperature points were distributed along the transversal and longitudinal axes of the combustion chamber with a spacing of 100 mm.

The transversal and longitudinal temperature profiles in the primary combustion zone are shown in Fig. 10 and Fig. 11, respectively. It was observed that the flame was symmetrically distributed along the central axis of the preheated fuel burner. The high-temperature primary combustion zone was mainly concentrated at 1100–2050 mm from the bottom of the combustion chamber, which was 200–400 mm away from the wall surface. In that region, temperatures were > 1150 °C; the peak temperature was 1256 °C at 1650 mm from the bottom of the combustion chamber. The flame assumed the shape of cone that diffused outward from the preheated fuel burner, exhibiting a length of 2300 mm and an I.D of 400 mm. A significant radial temperature gradient occurred below 2050 mm from the bottom of the combustion chamber, and the maximum radial temperature difference was 336 °C at 950 mm from the bottom of the combustion chamber. The high-speed jet of the secondary air flow resulted in a high radial velocity gradient in the region near the preheated fuel burner. Accordingly, the preheated fuel was

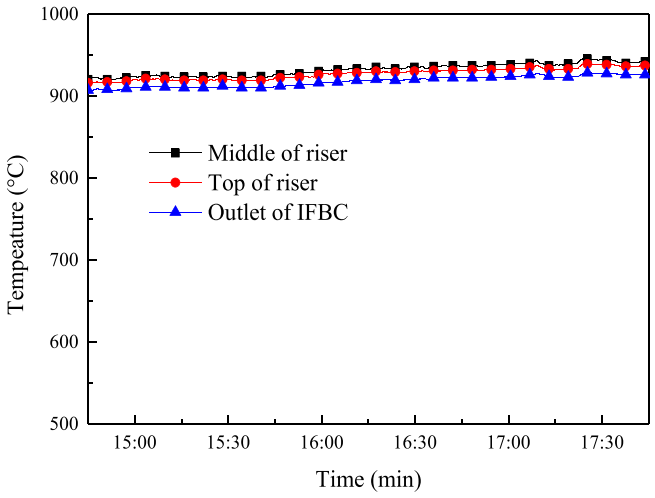

Fig. 8. Temperature variations with time in the IFBC.

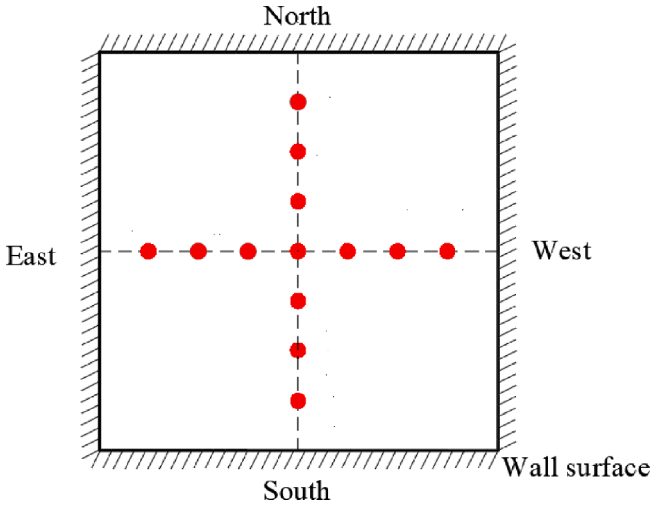

Fig. 9. The temperature points on the cross section of the combustion chamber.

Table 4
Analysis of high-temperature coal gas.

Item	unit	value
N_2	%	69.89
H_2	%	10.93
CO	%	12.21
CH_4	%	3.01
CO_2	%	3.85
O_2	%	0.00
C_mH_n	%	0.11
Low heating value	MJ/Nm^3	4.36

Table 5
Analysis of high-temperature semi-coke and the conversion rate of each component.

Items	Value	Conversion rate (%)
Ultimate analysis (wt %, air-dried basis)		
Carbon (C_{ad})	61.90	65.9
Hydrogen (H_{ad})	1.58	85.9
Oxygen (O_{ad})	6.30	78.5
Nitrogen (N_{ad})	0.56	80.2
Sulfur (S_{ad})	1.02	11.5
Proximate analysis (wt %, air-dried basis)		
Moisture (M_{ad})	0.34	99.0
Ash (A_{ad})	28.30	0.00
Volatile matter (V_{ad})	1.96	97.8
Fixed carbon (FC_{ad})	69.40	49.6

wrapped and carried upward by secondary air. Thus, the fuel did not sufficiently mix and diffuse, and it was concentrated in the central area and was rapidly ignited to maintain a high flame temperature. As combustion chamber height was elevated, the mixing of reactants was strengthened as impacted by the decrease of radial velocity gradient and the entrainment of the surrounding flue gas. Thus, a more uniform temperature profile was obtained, and the radial temperature difference was < 150 °C at a location above 2050 mm from the bottom of the combustion chamber.

The experimental data along the axis of the combustion chamber (e.g., temperature, pressure, and CO or NO_x concentrations) were not sampled owing to limited experimental conditions. Refer to the previous researches [23–26], the following section did a simple analysis and discussion about the effects of M_{io} and tertiary air position using the air velocities of preheated fuel burner, the grid temperature measurement in the primary combustion zone, and the resulting NO_x emissions. In addition, a CFD-based calculation can provide more information on the flow, mixing, and chemical reaction inside the combustion chamber. Hence, the related numerical calculations will be addressed in future research.

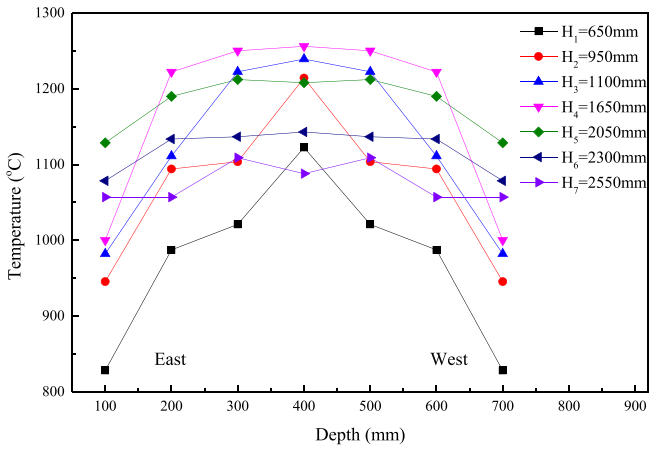

Fig. 10. Transversal temperature profiles in the primary combustion zone.

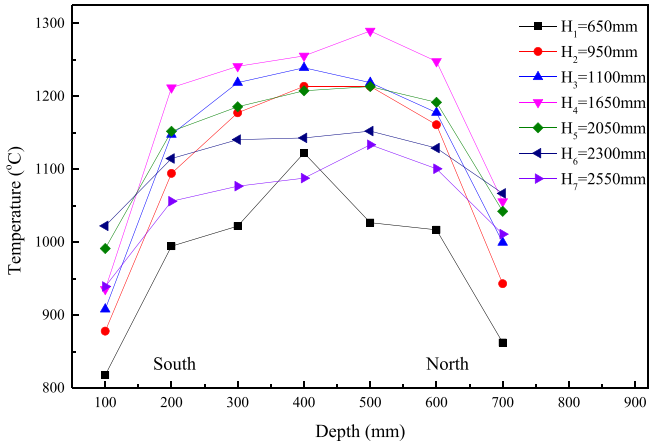

Fig. 11. Longitudinal temperature profiles in the primary combustion zone.

3.3. Effect of M_{io} on the combustion characteristics and NO_x emissions

To determine the effect of M_{io} on the combustion characteristics and NO_x emissions, comparative cases 2–4 were selected for discussion. M_{io} was 0.22, 0.39, and 0.62 for cases 2–4, respectively, considering that slight variations in thermal power, λ_p, λ_s, and λ_t were negligible. Tertiary air was supplied at 10700 mm from the bottom of the combustion chamber via nozzle 4.

Fig. 12 presents the temperature profiles along the axis of the combustion chamber at different M_{io}. The preheated fuel was first mixed with the ISA and burned to release heat, which indicated that M_{io} was critical to fuel mixing and reaction during the early-stage combustion. Notably, the high-temperature primary combustion zone moved upward with decreasing M_{io}. In cases 2–4, the peak temperature ranged from 1140 °C to 1160 °C, at the corresponding locations 2370, 1570, and 1160 mm from the bottom of the combustion chamber. The decrease of M_{io} indicated outer secondary air flow rate increased, and v_{out} increased accordingly. Consequently, more preheated fuel was carried upward, and the occurrence of the confluence point of the fuel and secondary air jet was delayed. In addition, the temperature in the region of 3000–8000 mm from the bottom of combustion chamber slightly increased with an increase of thermal power. In addition, the resulting temperature profiles were almost equivalent for cases 2–4 at a location above 8000 mm from the bottom of the combustion chamber, which demonstrated that the effect of M_{io} on late-stage combustion was negligible.

The peak temperature in the combustion chamber was < 1300 °C, and thus the thermal NO_x generation could be significantly inhibited [35,36]. In addition, prompt NO_x from the combustion of pulverized coal was rather low [37]. As volatile-N was almost entirely released during the preheating process, NO_x in the combustion chamber was mainly converted from char-N.

The mechanism of NO_x formation in the combustion chamber has been addressed through a bench-scale test rig, as reported by Ouyang [24,38]. Before the tertiary air injection into the chamber, the supplied air was inadequate. Hence, a reducing atmosphere prevailed in the area between the preheated fuel burner and the tertiary air nozzle. This zone was defined as the reducing zone, wherein a series of oxidation and reduction reactions occurred. The specific surface area of the solid fuel particle was enlarged after preheating in the IFBC, which represented an expanded reaction area [24]. In addition, H_2, CO, and C_nH_m contained in the high-temperature coal gas contributed to the reduction of NO_x. Thus, the generated NO_x was easily reduced through homogeneous reduction [39,40] and heterogeneous reduction [41].

Fig. 13 presents the variations in NO_x emissions and CO emissions at different M_{io}. At M_{io} of 0.22, 0.39, and 0.62, the resulting NO_x emissions were 150, 285, and 321 mg/Nm^3 (@6% O_2), respectively. CO emissions ranged from 129 mg/Nm^3 to 182 mg/Nm^3 (@6% O_2), and they were not the main factor affecting the NO_x emissions. NO_x emissions decreased apparently with the decrease in M_{io}, being reduced by 53.3% when M_{io} decreased from 0.62 to 0.22. M_{io}, which represents the relative flow rate of ISA and OSA at a fixed λ_s, allows for the assessment of the air staging ratio of the preheated fuel burner. The preheated fuel prematurely mixed with more oxygen during early-stage combustion at M_{io} of 0.62, which might have caused a local high-oxidation region that promoted NO_x generation. ISA decreased and OSA conversely increased with decreasing M_{io}, which indicated a deeper air staging of the preheated fuel burner. Accordingly, a low-oxygen region with strong reducibility was formed to inhibit NO_x generation. Notably, NO_x emissions decreased with decreasing of λ_s [23,26]. Both λ_s and M_{io} for Case 2 were lower than those for Case 3 and 4. Lower NO_x emissions in case 2 may have also been caused by the decrease in λ_s. The effect of M_{io} on NO_x

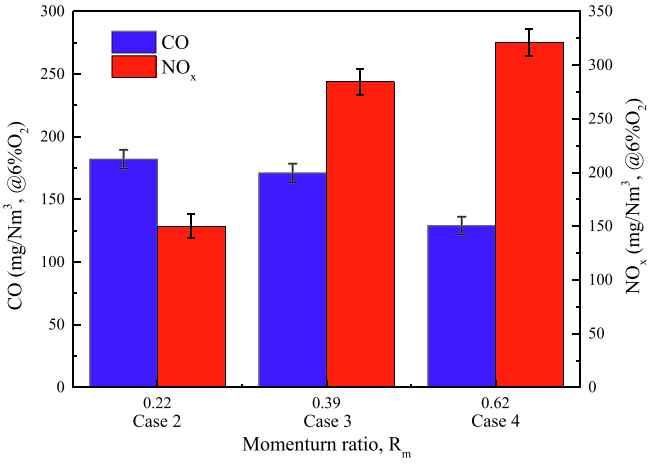

Fig. 13. NO_x emissions and CO emissions with different M_{io}.

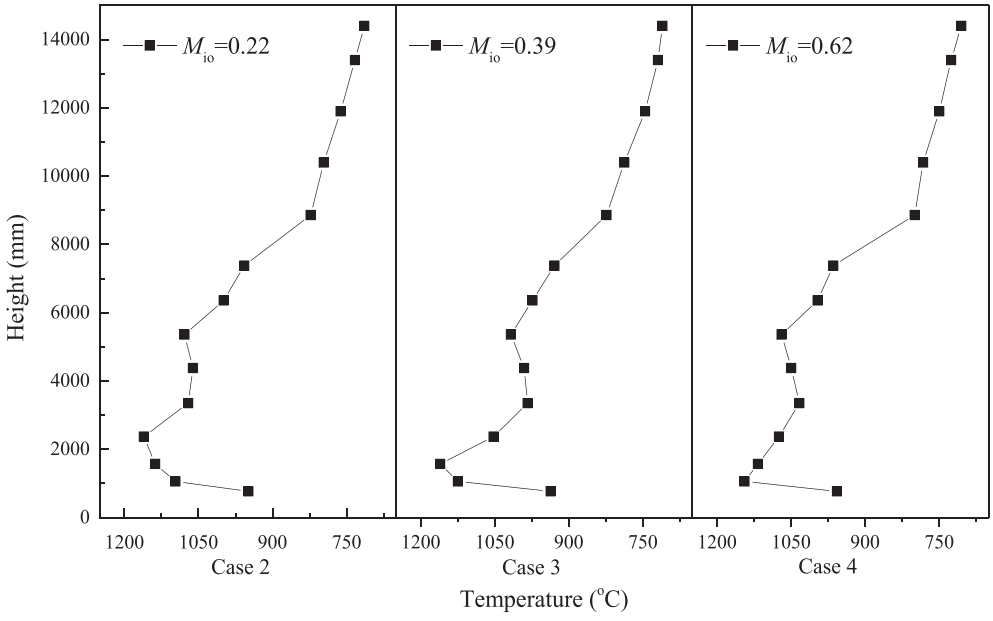

Fig. 12. . Temperature profiles along the axis of the combustion chamber with different M_{io}.

emission with a single characteristic quantity will be addressed in future research. Furthermore, v_{in} and v_{out} were 33 m/s and 56 m/s, respectively, at M_{io} of 0.22. In this case, the velocity gradient of the preheated fuel burner was not reasonable. The high shear stress of the high-speed jet flow hindered the radial mixing of the preheated fuel and air in the reducing zone. For this burner, the potential of coupling the strongly reducing atmosphere with strong turbulence was not fully exerted. Consequently, a strong turbulence structure should be introduced in the preheated fuel burner, which may further contribute toward reducing NO_x emissions.

3.4. Effect of the position of tertiary air on the combustion characteristics and NO_x emissions

To determine the effect of the position of tertiary air on the combustion characteristics and NO_x emissions, comparative cases 5–8 were selected for discussion. In case 5–8, tertiary air was supplied into the combustion chamber via nozzles 2 and 3, nozzles 3 and 4, nozzles 4 and 5, nozzle 5, respectively, while the thermal power, λ_p, λ_s, M_{io}, and λ_t remained constant.

Fig. 14 presents the temperature profiles along the axis of the combustion chamber at different tertiary air positions. The temperature profiles in cases 5–8 were similar at a location below 4500 mm from the bottom of the combustion chamber. The peak temperature ranged from 1240 °C to 1270 °C at approximately 1000 mm from the bottom of the combustion chamber. The effects of the slight variations in thermal power, λ_p, λ_s, and M_{io} on the temperature profile along the combustion chamber were considered negligible. However, the position of the tertiary air was crucial for the temperature profiles during the late-stage combustion. Once the tertiary air was injected into the combustion chamber, the preheated fuel was rapidly burned and the temperature increased. For instance, tertiary air was fed into the combustion chamber via nozzles 2 and 3 in case 5, and the temperature increased rapidly at 5000–9000 mm from the bottom of the combustion chamber. Thus, the temperature profile in the combustion chamber could be modified by reasonably adjusting the tertiary air flow.

Fig. 15 presents the NO_x and CO emissions at different positions of the tertiary air. CO emissions were < 100 mg/Nm^3 overall (@ 6% O_2). NO_x emissions were 140, 78, and 72 mg/Nm^3 (@ 6% O_2) in cases 5–7, respectively, (corresponding to nozzles 2 and 3, nozzles 3 and 4, nozzles 4 and 5). This indicated that NO_x emissions could be effectively reduced by the delayed injection of tertiary air. The reducing zone expanded as the height of the tertiary air nozzle increased, indicating that the retention time of the reactants in the reducing zone also increased.

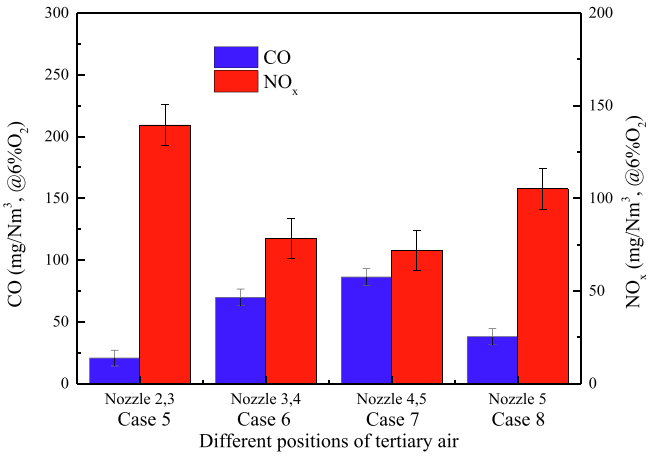

Fig. 15. NO_x emissions and CO emissions with different positions of tertiary air.

Hence, the NO_x reduction reaction was more sufficient accordingly. This conclusion complied with the study reported by Man [23]. The decrease in NO_x emissions in Case 7 (compared with cases 5 and 6) might have also been caused by the decrease in λ_s [23,26]. The effect of tertiary air position will be clarified further in our future study. In addition, NO_x emissions increased to 105 mg/Nm^3 (@ 6% O_2) for Case 8. Though the reducing zone expanded further with nozzle 5, tertiary air was injected into the combustion chamber through only one nozzle. This indicated that the preheated fuel mixed with a large amount of oxygen in a relatively small space, leading to the formation of a local high-oxidation region close to nozzle 5. Hence, a large amount of NO_x was generated and could hardly be reduced because it was no longer a strongly reducing atmosphere. Liu [29] reported that a uniform combustion reaction and low oxygen concentration were conducive to inhibiting the generation of NO_x, which was supported by the experimentally achieved result. The tertiary air that was fed through nozzles 4 and 5 in Case 7 could disperse into a larger space compared to that in Case 8, and thus formed a sufficiently low-oxygen atmosphere throughout the combustion chamber. Accordingly, the preheated fuel mixed with oxygen well and the reactions could occurred uniformly in the combustion chamber. Consequently, NO_x emissions in Case 7 decreased. In summary, the long retention time in the reducing zone and the uniform mixing of reactants are critical for the reduction of NO_x emissions. Further, the multi-layer arrangement and delayed supply of tertiary air facilitated the

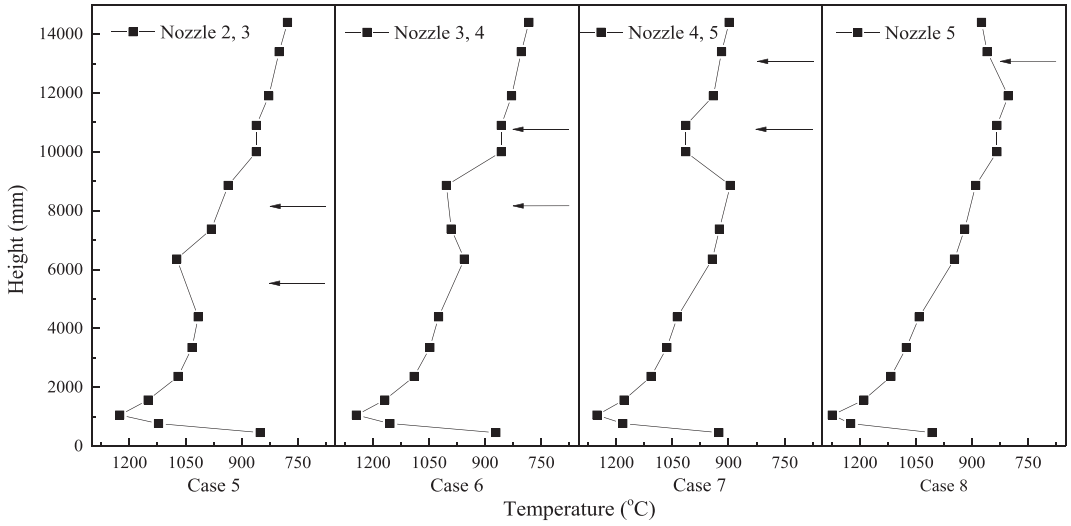

Fig. 14. Temperature profiles along the axis of the combustion chamber with different tertiary air positions.

reduction of NO_x emissions.

3.5. Combustion efficiency

The coal preheating technology demonstrated excellent performance in terms of combustion efficiency [25,31]. In this study, the combustion efficiency of chosen typical case (cases 6 and 8) was investigated. The combustion efficiency was calculated as follows [23]:

$$\eta = 1 - q_s - q_g \quad (7)$$

$$q_s = \frac{32700 A_{ar} C_{fa}}{Q_{net,ar}(100 - C_{fa})}, \% \quad (8)$$

$$q_g = 236(C_{ar} + 0.375 S_{ar}) \frac{CO}{RO_2 + CO} \cdot \frac{100 - q_s}{Q_{net,ar}}, \% \quad (9)$$

where η is the combustion efficiency, q_s is the heat loss due to incomplete combustion of the solid combustibles (mainly carbon), $Q_{net,ar}$ is the net calorific value of the as-received fuel, A_{ar} is the mass fraction of the ash in the as-received fuel, C_{fa} is the combustible content in the exit fly ash, q_g is the heat loss due to incomplete combustion gases (mainly CO), CO is the volumetric percentage of CO in the dry flue gas, and RO_2 is the volumetric percentage of triatomic gas in the dry flue gas.

The fly ash at the inlet of the bag filter was sampled using a filter cartridge via a vacuum pump. In cases 6 and 8, the C_{fa} fractions were 2.41% and 6.32%, respectively, and the corresponding combustion efficiencies were 99.1% and 97.6%, respectively. The average combustion efficiency of the Shenmu bituminous coal was 98.4%.

Efficient and clean utilization of pulverized coal was achieved using a 2 MW novel self-sustained preheating combustion test rig. There may exist two development routes for its industrial application: the scale up of each combined IFBC and furnace unit, and a combination of several IFBC units with existing pulverized coal boiler. Further research and numerical calculations are required to address crucial issues such as the design criteria of the IFBC, the wear under long-term operation, and coupling between the IFBC and the furnace. The industrial application of the coal self-sustained preheating combustion technology has the potential to be realized in the future.

4. Conclusion

In this study, the high combustion efficiency and low-NO_x emissions control were addressed. An experiment was performed in a 2 MW novel self-sustained preheating combustion test rig to investigate the NO_x emissions and combustion characteristics using bituminous coal. The effects of the air staging ratio of the preheated fuel burner and the position of tertiary air were studied. Moreover, the preheating characteristics of the IFBC and the temperature profile in the primary combustion zone were investigated. The main findings are summarized as follows:

1. Pulverized coal can be efficiently and cleanly used through self-sustained preheating combustion technology. NO_x emissions decreased to 72 mg/Nm^3 (@ 6% O_2), while a high combustion efficiency of 98.4% was achieved.
2. IFBC can provide the high-temperature preheated fuel for the combustion chamber stably. The conversion rate of the fuel-N reached up to 80.2% in the IFBC, conducive to inhibiting NO_x generation.
3. The high-temperature primary combustion zone was concentrated at 1100–2050 mm from the bottom of the combustion chamber. The corresponding temperature profile exhibited a symmetrical distribution along the central axis of the preheated fuel burner.
4. The air staging ratio of the preheated fuel burner is critical for the mixing process and reaction of the preheated fuel during early-stage combustion. The high-temperature primary combustion zone moved upward with decreasing M_{io}. This contributed to the formation of a low-oxygen region with strong reducibility, leading to the efficient reduction of NO_x.
5. A comprehensive approach on low NOx emissions required a long retention time in the reducing zone and uniform mixing of the reactants. The multi-layer arrangement and delayed supply of the tertiary air facilitated the reduction of NO_x emissions.

CRediT authorship contribution statement

Ziqu Ouyang: Methodology, Validation, Formal analysis, Investigation, Writing - review & editing. **Wenhao Song:** Formal analysis, Investigation, Writing - original draft, Visualization. **Jingzhang Liu:** Methodology, Validation, Formal analysis, Investigation, Writing - original draft, Visualization. **Jianguo Zhu:** Conceptualization, Supervision, Project administration, Funding acquisition. **Chengbo Man:** Investigation. **Shujun Zhu:** Investigation. **Hongliang Ding:** Investigation.

Declaration of Competing Interest

The authors declare that they have no known competing financial interests or personal relationships that could have appeared to influence the work reported in this paper.

Acknowledgments

This study was supported by the National Key R&D Program of China (2017YFB0602001); Youth Innovation Promotion Association, Chinese Academy of Sciences (2019148).

References

[1] National Standards of People's Republic of China: emission standard of air pollutants for thermal power plants, GB 13223–2011. http://pro0afb79.pic38.websiteonline.cn/upload/ha8g.pdf.
[2] DIRECTIVE 2001/80/EC OF THE EUROPEAN PARLIAMENT AND OF THE COUNCIL of 23 October 2001 on the limitation of emissions of certain pollutants into the airfrom large combustion plants. https://eur-lex.europa.eu/LexUriServ/LexUriServ.do?uri=CONSLEG:2001L0080:20070101:EN:PDF.
[3] Hodžić N, Kazagić A, Smajević I. Influence of multiple air staging and reburning on NOx emissions during co-firing of low rank brown coal with woody biomass and natural gas. Appl Energy 2016;168:38–47.
[4] Liu C, Hui S, Pan S, Wang D, Shang T, Liang L. The influence of air distribution on gas-fired coal preheating method for NO emissions reduction. Fuel 2015;139:206–12.
[5] Fan W, Lin Z, Kuang J, Li Y. Impact of air staging along furnace height on NOx emissions from pulverized coal combustion. Fuel Process Technol 2010;91:625–34.
[6] Zeng L, Li Z, Zhao G, Li J, Zhang F, Shen S, et al. The influence of swirl burner structure on the gas/particle flow characteristics. Energy 2011;36:6184–94.
[7] Zhou C, Wang Y, Jin Q, Chen Q, Zhou Y. Mechanism analysis on the pulverized coal combustion flame stability and NOx emission in a swirl burner with deep air staging. J Energy Inst 2018;92:298–310.
[8] Daood SS, Javed MT, Gibbs BM, Nimmo W. NOx control in coal combustion by combining biomass co-firing, oxygen enrichment and SNCR. Fuel 2013;105:283–92.
[9] Wu CF, Nahil MA, Sun X, Singh S, Chen JH, Shen BX, et al. Novel application of biochar from biomass pyrolysis for low temperature selective catalytic reduction. J Energy Inst 2012;4:236–9.
[10] Nimmo W, Javed MT, Gibbs BM. NOx control by ammonium carbonate and ammonia with hydrocarbons as additives. J Inst Energy 2008;3:131–4.
[11] Der Lans RPV, Glarborg P, Damjohansen K. Influence of process parameters on nitrogen oxide formation in pulverized coal burners. Prog Energy Combust Sci 1997;23:349–77.
[12] Ukeguchi Y, Sakai K, Kokuryo S, Saito K, Suto T, Yamashita T. Mitsubishi Hitachi Power Systems Ltd. Boiler Business and Technology Development. Mitsubishi Heavy Industries Technical Review, 2015, 52: 55-63.
[13] Chen Z, Li Z, Wang F, Jing J, Chen L, Wu S. Gas/particle flow characteristics of a centrally fuel rich swirl coal combustion burner. Fuel 2008;87:2102–10.
[14] Zhao L, Zhou Q, Zhao C. Flame characteristics in a novel petal swirl burner. Combust Flame 2008;155:277–88.
[15] Moon C, Sung Y, Eom S, Choi G. NOx emissions and burnout characteristics of bituminous coal, lignite, and their blends in a pulverized coal-fired furnace. Experimental Thermal Fluid Sci 2015;62:99–108.
[16] Sung Y, Moon C, Eom S, Choi G, Kim D. Coal-particle size effects on NO reduction and burnout characteristics with air-staged combustion in a pulverized coal-fired furnace. Fuel 2016;182:558–67.

[17] Li Y, Fan W. Effect of char gasification on NOx formation process in the deep air-staged combustion in a 20 kW down flame furnace. Appl Energy 2016;164:258–67.
[18] Fan W, Li Y, Guo Q, Chen C, Wang Y. Coal-nitrogen release and NOx evolution in the oxidant-staged combustion of coal. Energy 2017;125:417–26.
[19] Kuang M, Li Z, Ling Z, Zeng X. Evaluation of staged air and overfire air in regulating air-staging conditions within a large-scale down-fired furnace. Appl Therm Eng 2014;67:97–105.
[20] Zha Q, Li D, Wang C, Che D. Numerical evaluation of heat transfer and NOx emissions under deep-air-staging conditions within a 600 MWe tangentially fired pulverized-coal boiler. Appl Therm Eng 2017;116:170–81.
[21] Liu C, Hui S, Zhang X, Wang D, Zhuang H, Wang X. Influence of type of burner on NO emissions for pulverized coal preheating method. Appl Therm Eng 2015;85:278–86.
[22] Lu Q, Zhu J, Niu T, Song G, Na Y. Pulverized coal combustion and No(x) emissions in high temperature air from circulating fluidized bed. Fuel Process Technol 2008;89:1186–92.
[23] Man C, Zhu J, Ouyang Z, Liu J, Lyu Q. Experimental study on combustion characteristics of pulverized coal preheated in a circulating fluidized bed. Fuel Process Technol 2018;172:72–8.
[24] Ouyang Z, Zhu J, Lu Q. Experimental study on preheating and combustion characteristics of pulverized anthracite coal. Fuel 2013;113:122–7.
[25] Zhu S, Lyu Q, Zhu J, Wu H, Wu G. Effect of air distribution on NO x emissions of pulverized coal and char combustion preheated by a circulating fluidized bed. Energy Fuels 2018;32:7909–15.
[26] Liu W, Ouyang Z, Cao X, Na Y. The influence of air-stage method on flameless combustion of coal gasification fly ash with coal self-preheating technology. Fuel 2019;235:1368–76.
[27] Song W, Li S, Ouyang Z. Operational performance characteristics of a novel fluidized bed with the internal separator for pulverized coal self-sustained preheating. Powder Technol 2020;361:782–90.
[28] Blondeau, Kock, Mertens, Eley, AJ, Holub. Online monitoring of coal particle size and flow distribution in coal-fired power plants: Dynamic effects of a varying mill classifier speed. Applied Thermal Engineering, 2016, 98: 449-454.
[29] Liu W, Ouyang Z, Cao X, Na Y, Liu D, Zhu S. Effects of secondary air velocity on NO emission with coal preheating technology. Fuel 2019;256:115898.
[30] Zhu J, Ouyang Z, Lu Q. An experimental study on NO x emissions in combustion of pulverized coal preheated in a circulating fluidized bed. Energy Fuels 2013;27:7724–9.
[31] Zhu S, Lyu Q, Zhu J, Liang C. Experimental study on NOx emissions of pulverized bituminous coal combustion preheated by a circulating fluidized bed. J Energy Inst 2019;92:247–56.
[32] Zhang Y, Zhu J, Lyu Q, Liu J, Zhang J. The ultra-low NOx emission characteristics of pulverized coal combustion after high temperature preheating. Fuel 2020;277:118050.
[33] Calkins WH. The chemical forms of sulfur in coal: a review. Fuel 1994;73:475–84.
[34] Li S, Xu T, Sun P, Zhou Q, Tan H, Hui S. NOx and SOx emissions of a high sulfur self-retention coal during air-staged combustion. Fuel 2008;87:723–31.
[35] Katsuki M, Hasegawa T. The science and technology of combustion in highly preheated air. Symp (Int) Combust 1998;27:3135–46.
[36] Fan W, Lin Z, Li Y, Li Y. Effect of Temperature on NO Release during the Combustion of Coals with Different Ranks. Energy Fuels 2010;24:1573–83.
[37] Hayhurst A, Vince I. Nitric oxide formation from N2 in flames: the importance of "prompt" NO. Prog Energy Combust Sci 1980;6:35–51.
[38] Ouyang Z, Liu W, Zhu J. Flameless Combustion Behaviour of Preheated Pulverized Coal. Can J Chem Eng 2018;96:1062–90.
[39] Furusawa T, Tsunoda M, Tsujimura M, Adschiri T. Nitric oxide reduction by char and carbon monoxide: fundamental kinetics of nitric oxide reduction in fluidizedbed combustion of coal. Fuel 1985;64:1306–9.
[40] Mei L, Lu X, Wang Q, Pan Z, Ji YHX. The experimental study of fly ash recirculation combustion characteristics on a circulating fluidized bed combustor. Fuel Process Technol 2014;118:192–9.
[41] Zhong B, Shi W, Fu W. Effects of fuel characteristics on the NO reduction during the reburning with coals. Fuel Process Technol 2002;79:93–106.